Continuum Theory for Wet Active Matter: Self-Propelled Rods in Stokes Fluids via Boltzmann-Ginzburg-Landau

Supervisors:
Alexandre Solon, LPTMC
Hugues Chaté, CEA-Saclay
Alessandro Pelizzola, PoliTO

Candidate:
Elia Bronzo

MSc Physics of Complex Systems - International track

Politecnico di Torino - July 2024

A.a. 2023/2024

Abstract

Active systems, ensembles of active particles capable of expending energy at the individual level to produce motion or other forms of mechanical work, are present at all scales in biology. Bacteria are a paradigmatic example of such out-of-equilibrium systems, as they can convert chemical energy into motion through structures such as pili or flagella.

Active turbulence is one possible state of collective motion exhibited by species of elongated and flagellated bacteria. Their rod-shaped bodies promote nematic alignment, leading to a so-called active nematics where nematic order is disrupted by the turbulent motion of topological defects.

A crucial ingredient to produce such collective motion is the effect of the fluid surrounding the bacteria. Indeed, even if they are too packed to swim, they set the fluid in motion which in turn lead to their chaotic swirling motion. Such behavior is well-reproduced by microscopic models of particles coupled to a fluid but, so far, we lack a coarse-grained continuum theory that would express the large-scale behavior in terms of the microscopic parameters.

In this work, we derive such a hydrodynamic theory for self-propelled rods embedded in a Stokes fluid by adapting the Boltzmann-Ginzburg-Landau approach, previously used in the dry case [12], to obtain a continuum theory from a wet microscopic model, including explicitly the fluid. This framework accounts for the complex interplay between self-propulsion, nematic alignment, and fluid dynamics.

Finally, we analyze the derived model by performing a linear stability analysis of the nematically ordered stationary homogeneous solution and numerically integrating the PDEs. This allows us to investigate the effects of the fluid on both the phase diagram and the non-linear dynamics, providing new insights into the behavior of this wet active matter model.

Keywords: active matter, self-propelled rods, out-of-equilibrium statistical physics, bacterial swarming, active nematics, active turbulence, hydrodynamic theory, Boltzmann-Ginzburg-Landau

Contents

Chapter 1

Introduction

1.1 What is active matter?

Active matter refers to systems composed of a large number of individual agents, each capable of converting stored or ambient free energy into motion or mechanical work. These systems are hence driven out of equilibrium at the level of their individual constituents,and constitute a different class of systems compared to systems that are driven out-of-equilibrium by the presence of an external field or from the boundaries. These agents, usually called *active particles*, are present at all scales in Biology, from the animal world (flocks of birds and schools of fish), to cells (bacterial and sperm suspensions) and inside cells (molecular motors and the cytoskeleton network). What is common to all these instances is the capacity to *self-organize* and give rise to various forms of *collective motion* at the macroscopic level (figure 1.1).

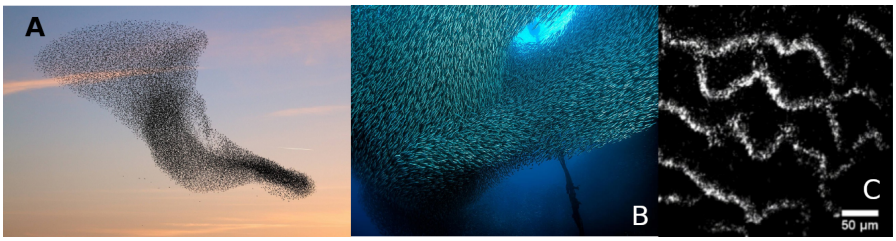

Figure 1.1: Examples of active systems exhibiting collective motion: (A) flocks of starlings [2], (B) schools of sardines, (C) bands in systems of actin filaments [14]

There are also examples of synthetic active systems often made of micrometric beads that can be activated by electric fields, light or chemical processes (figure 1.2).

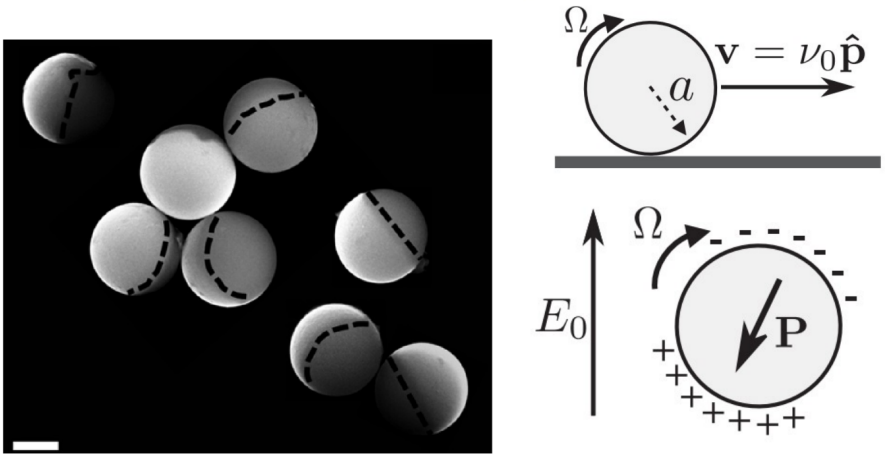

Figure 1.2: Examples of synthetic active systems. *Left*: Janus colloids are micrometer-size silica beads half-coated with a nanometer-thick Platinum film that is able to catalyze the reaction of H_2O_2. When in solution, the reaction takes place only on one side of the colloid leading to a gradient of concentration that propels the particle diffusiophoresis [18]*Right*: Quincke rollers consist of insulating beads immersed in a conducting fluid. Applying an electric field in the vertical direction results in surface-charge dipoles whose orientation is unstable for large enough field leading to a rolling motion of the beads in the horizontal plane. [5]

1.2 Active Turbulence

Active agents immersed in a fluid create a so-called *active fluid* that can exhibit spontaneous flow with a complex spatiotemporal structure. Such complex fluids can be physically realised in different ways starting from active biological agents (bacterial suspensions, sperm cells, cytoskeletal suspensions) but also engineered self-propelled colloids (Janus particles). Even if at low Reynolds, these systems exhibit chaotic flows reminiscent of inertial turbulence which inspired the name *active turbulence* for such phenomena. A few physical systems manifesting active turbulence are shown in figure 1.3.

The motivation for my project is to understand the behaviour of bacterial swarms. Swarming, most often observed in rod-shaped flagellated bacterial species moving on a substrate, is a collective mode of motion in which such species can transition into and it is characterized by chaotic whirls and jets and it is a prominent example of active turbulence in quasi-2D geometries. The type of collective motion of interest in my project is the so called bacteria's *swarming* (figure 1.4). This is a collective mode of motion in which some bacterial species, usually rod-shaped and flagellated, can transition into and is characterized by a fast migration

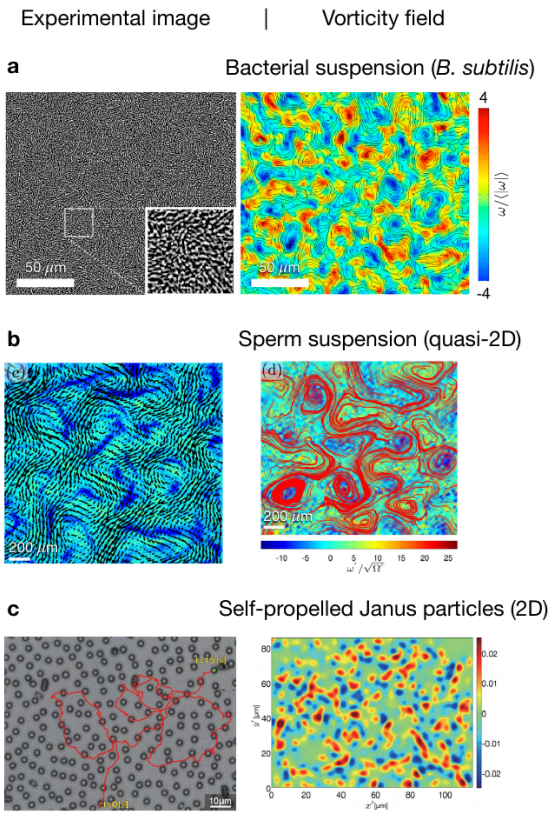

Figure 1.3: Examples of active turbulence in different biological and artificial active systems taken from [1].

over surfaces and the formation of dynamic patterns of whirls and jets [3], two types of motion that can also be described as active turbulence.

1.3 Dry models of active matter

Different models of active matter systems have been proposed depending on the type of interaction between the particles. In the simplest case, the fluid that surrounds the particles is not taken into account. In such dry models one of the possible distinction that can be made is between *scalar* and *aligning* active matter. This difference is in the capacity or not, for the models' particles, to change their orientation in space depending on the orientation of other (usually neighbors') particles. Others forms of interaction can be considered in both cases leading to an interesting collective behaviour.

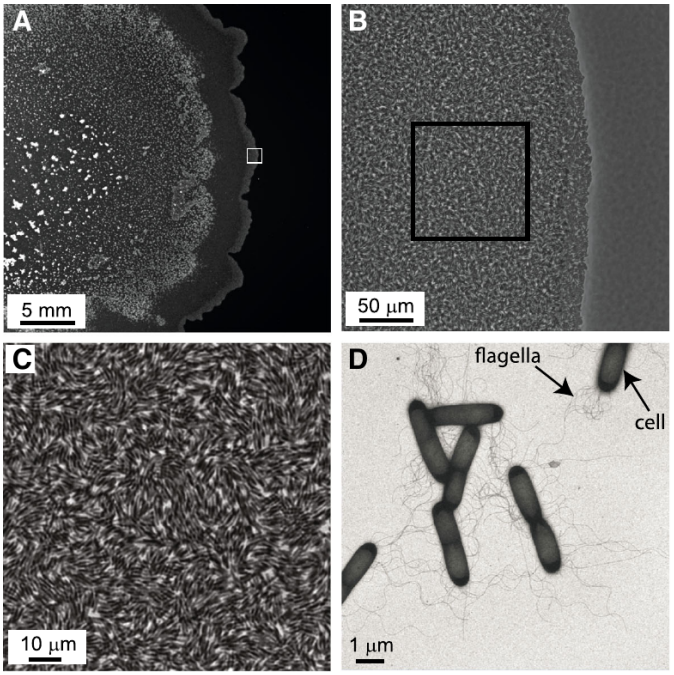

Figure 1.4: (A,B,C): Different level of magnification of a swarming colony, (B,C) focus on the active part of the bacteria colony. (D) TEM image of typical swarming bacteria, elongated bodies and flagella. [3]

Scalar active matter and MIPS

One typical phenomenon that can be found in scalar active matter and does not have an equivalent at equilibrium is the so called Motility Induced Phase Separation (MIPS) [13]. A minimal model for scalar active particles that undergoes MIPS consists of Active Brownian Particles (ABP are self propelled particles whose orientation undergoes a diffusive dynamic) interacting via steric repulsion. MIPS takes place because collisions between particles effectively reduce their speed in denser regions and in returns particles tend to accumulate in regions where their velocity is slower leading to a positive feedback loop. What is observed is the presence of dense "liquid" regions in which particles move slower surrounded by dilute gas characterized by a faster motion of the particles as can be seen in figure(1.5).

Aligning active matter: Vicsek model

Probably the most important example of aligning active matter is the model introduced in 1995 in the celebrated paper by Vicsek and collaborators [17]. The model contains only alignement and self propulsion and consists in a simple discrete-time dynamics in which N point-like particles move at constant speed v_0 in a periodic

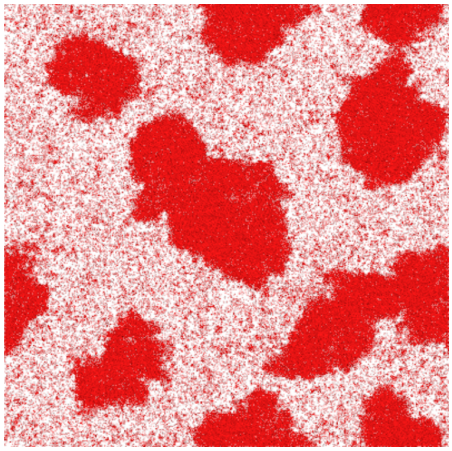

Figure 1.5: Motility Induced phase separation from numerical simulation of ABPs with steric repulsion [13]

2D domain and interact via a local alignment rule in the presence of angular noise. In terms of equations:

$$\vec{r}_i^{\,t+1} = \vec{r}_i^{\,t} + v_0 \hat{e}(\theta_i^{t+1}), \tag{1.1}$$

$$\theta_i^{t+1} = \mathrm{Arg}\left[\langle \hat{e}(\theta_j^t)\rangle_i\right] + \xi_i(\eta) \tag{1.2}$$

Where ξ is a uniform white noise sampled from $[-\frac{\eta}{2}, \frac{\eta}{2}]$ with η its strength, and $\langle\cdot\rangle_i$ is the mean computed for the particles within a radius r_0 from particle i figure 1.6a. Applying this rule at large noise and/or low density results in a disordered phase in which there is no net motion of the particles. Increasing the density or decreasing noise leads to an ordered phase in which all the particles move collectively in the same direction. In the density-noise phase diagram (figure 1.6b) there is also an intermediate region characterized by the coexistence of the two phases. Some dense, ordered regions also called *bands* since they posses an elongated structure and in particular their direction of motion is transversal to their axis (figure1.6c) move in a disordered "gas".

The starting point to model the behaviour of bacteria in swarming colonies is a microscopic Vicsek-like model but with a few differences described in the following.

1.3.1 Self-propelled rods

The bacteria under consideration in our case are characterized by the presence *rotating flagella* and an *elongated body*. The former provides a self propulsion speed while the latter provides the direction in which the bacterium moves. Furthermore, the elongated shape, provides a reason to believe that such elongated objects when they interact (e.g. upon collision) tends to align in either directions compatible

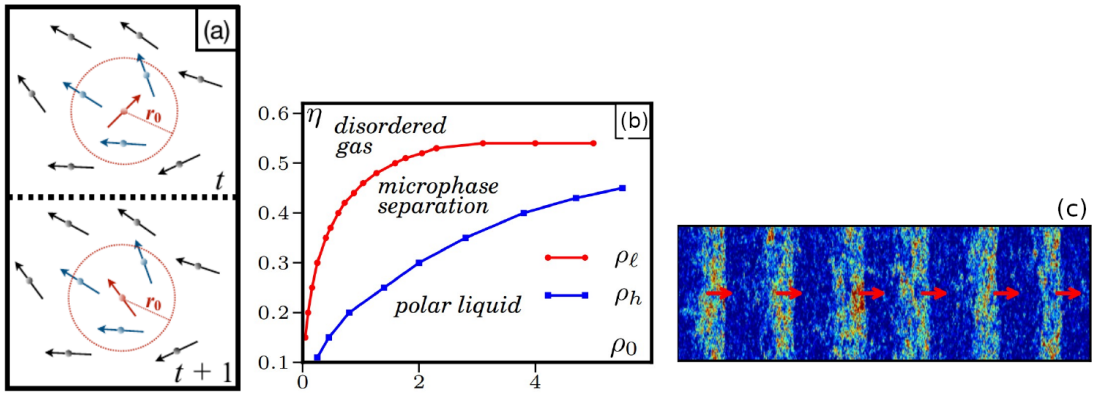

Figure 1.6: (a): Illustration of the Vicsek alignment rule, the red particle adjust is orientation according to the orientation of the neighbors (blue) particles within an interaction radius r_0. [10] (b): Phase diagram of the Vicsek model in the mean density ρ_0 and noise η plane from [15]. (c): Snapshot of bands solutions in the Vicsek model, color indicates density, arrows indicate direction of propagation. [15]

with their elongated body leading to a so-called *nematic* alignment (see figure 1.7) For this kind of particles, we can think a Vicsek-like model, still made of particles with polar self-propulsion but aligning locally with a nematic alignment rule. These active particles are usually called *self-propelled rods* and are used in this work as a microscopic starting model for the bacteria. This microscopic model has been shown to be capable of sustaining nematic order at low enough noise and also chaotic nematically ordered bands for intermediate noise's intensities [6] as can be seen in figure 1.8.

Hydrodynamic theories

Insights on the behaviour of this kind of microscopic models can only be provided by an hydrodynamic theory. This is an continuum description of the statistical properties of our system in the form of a set of PDEs for the *slow variables* of the system. There are two types of slow variables: those related to conserved quantities, in our case the density ρ, and those associated to symmetry breaking,

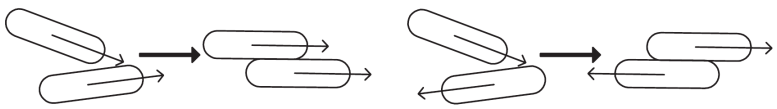

Figure 1.7: Illustration of nematic alignment for elongated objects after collisions [6]

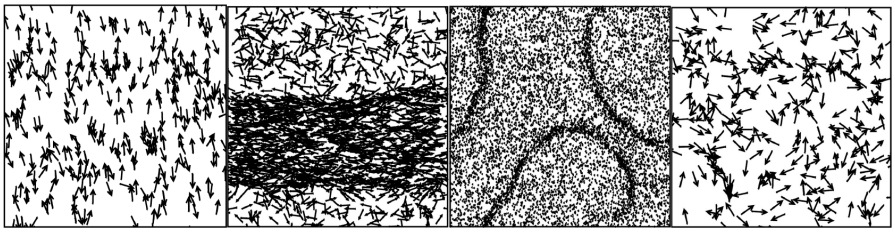

Figure 1.8: Different phases from simulations of the Dry microscopic model of self-propelled rods. Particles represented as arrows indicating their orientation exept in the third from the left. From left to right, increasing the noise we have respectively: quasi-long range nematic order, stable nematically ordered bands, chaotic nematically ordered bands, disordered phase. Taken from [6]

the polarity and/or the nematic tensor:

$$\vec{p} = \begin{pmatrix} \langle \cos\theta \rangle \\ \langle \sin\theta \rangle \end{pmatrix} \qquad \mathbf{Q} = \begin{pmatrix} \langle \cos 2\theta \rangle & \langle \sin 2\theta \rangle \\ \langle \sin 2\theta \rangle & -\langle \cos 2\theta \rangle \end{pmatrix} \tag{1.3}$$

An hydrodynamic theory for the original Vicsek model was first written on symmetry arguments by Toner and Tu [16]. The relevant hydrodynamic fields for this system are the coarse-grained density $\rho(\vec{r},t)$ and polarity $\vec{p}(\vec{r},t)$ and satisfy:

$$\partial_t \rho + v_0 \vec{\nabla} \cdot (\rho \vec{p}) = 0 \tag{1.4}$$

$$\partial_t \vec{p} + \lambda_1 (\vec{p} \cdot \vec{\nabla}) \vec{p} + \lambda_2 (\vec{\nabla} \cdot \vec{p}) \vec{p} + \lambda_3 \vec{\nabla} (|\vec{p}|^2) = (\alpha - \beta |\vec{p}|^2) \vec{p} - \vec{\nabla} P + D_I \Delta \vec{p} + D_A \vec{\nabla} (\vec{\nabla} \cdot \vec{p}) + \vec{f} \tag{1.5}$$

Equation 1.4 is the usual continuity equation for the density field. The first term on RHS of equation 1.5 is a Ginzburg-Landau term responsible, at low enough noise or large enough density (both α and β positive), for an homogeneous polarly ordered solution:

$$\rho = \rho_0 \quad ; \quad \vec{p} = \vec{p_0} = \sqrt{\frac{\alpha}{\beta}} \hat{e} \tag{1.6}$$

and $\vec{f}$ is an additive gaussian noise.

The phenomenological nature of these equations means that *a priori* all possible 7 coefficients and the pressure P are arbitrary functions of the microscopic parameters ρ and $\vec{p}$ and cannot be estimated with this approach. This make difficult to explore all the parameter space if not impossible to do a proper study of the phase diagram.

Other approaches have been developed to obtain hydrodynamic equations directly coarse-graining Vicsek-like microscopic models that also make possible to

obtain expressions of the theory's coefficients in terms of the microscopic ones. One of these methods is called *Boltzmann-Ginzburg-Landau* and it will be described in depth in the following and used to derive an hydrodynamic theory for the system under study.

1.4 Wet Vicsek-like model for active turbulence

The internship is devoted to model quasi-2D densely packed swarming bacteria suspensions. A microscopic model for this kind of systems has been proposed and studied in (H.Li *et al.* [9]) to describe the motion in swarming colonies of *Serratia Marscences*. This species is characterized by an elongated body and rotating flagella similar to figure (1.4d) and shows the characteristic behaviour of *active nematics* in which active turbulence happens because of the chaotic motion of topological defects with nematic symmetry (figure 1.9). Two kind of defects can be observed: $-\frac{1}{2}$ defects characterized by their threefold rotationally symmetric structure and $+\frac{1}{2}$ defects characterized by a polar structure. The number associated to each kind of defects, also known as their charge, is the winding number, that measure the change in orientation in the nematic field as a closed loop is traversed around the center of the defects.

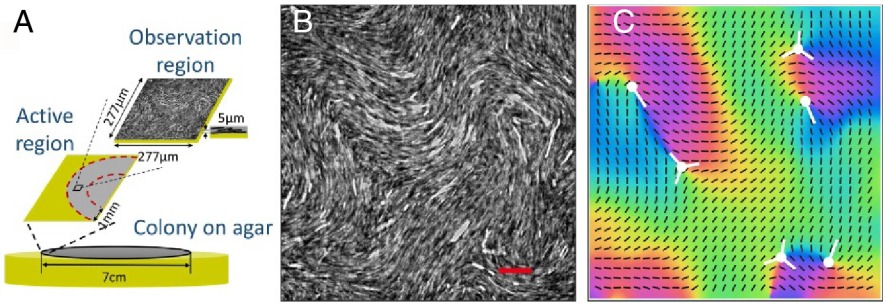

Figure 1.9: Active Nematics experimental observations on *Serratia Marscences*, adapted from [9]. (A) Illustration of a typical colony growing on an agar plate, the observation are made in the active region at the border of the colony. (B) Raw image of fluorescent cells (scale 30μm). (C) Nematic field and defects' positions and orientations extracted from B.

Such microscopic model, after tuning its parameters, was able to reproduce with an high level of accuracy the statistical properties of the swarming such as velocity and orientation correlation length, correlation time and defects speed.

The model consists in a minimal Vicsek-like model, in which self-propelled rods are embedded in a Stokes fluid whose interaction with the particles are explicitly

modeled (what is called a *Wet* active matter model). The fluid in this case is essential to explain the behaviour of the particles, since they are capable of applying a force on the fluid putting it in motion. The fluid then further rotates and advects the particles leading to the complex patterns observed experimentally. As shown in (H.Li *et al.*) the fluid is essential to model correctly such motion. Strikingly, even when considering self-propelled rods without self-propulsion (the bacteria may be unable to actually "swim" in the fluid since are to packed) they are still able to put the fluid in motion which is then responsible for active turbulence on the large scale.

At the same time a proper hydrodynamic theory for such wet active matter models is still missing hence the aim of the internship is to derive a continuum theory from a microscopic model similar to the one proposed in H.Li *et al.* with the Boltzmann-Ginzburg-Landau approach. The starting point will be the following overdumped dynamic coupled to a Stokes equation:

$$\dot{\vec{r}_i} = s_0 \hat{e}(\theta_i) + \vec{v}(\vec{r}_i) \tag{1.7}$$

$$\dot{\theta}_i = C_a \sum_{j\sim i} \sin[2(\theta_i - \theta_j)] + C_v(\vec{\nabla} \times \vec{v}) \cdot \hat{z} + C_s \hat{u}_i \times (\mathbf{E} \cdot \hat{u}_i) \cdot \hat{z} + C_n \xi_\theta \tag{1.8}$$

$$\mu \nabla^2 \vec{v} + \nabla P - \alpha \vec{v} + g_0 \vec{p} - f_d \nabla \cdot \mathbf{Q} = 0 \quad \text{with} \quad \nabla \cdot \vec{v} = 0 \tag{1.9}$$

The equation eq. (1.7) contains two contributions to particle's velocity, the first coming from the self propulsion speed and the second from advection by the fluid. The first term on the RHS of eq. (1.8) is a torque providing nematic alignment with the neighbors. Then we have two terms that summarize the effect of the fluid on the particles orientation with C_v and C_s being Jeffrey coefficients for the vorticity and strain rate whose value may differ from the one computed for perfect ellipsoids [8]. ξ_θ is a Gaussian white noise with strength C_n. Finally eq. (1.9) is the Stokes equation for the fluid with μ the viscosity and α an effective friction coefficient with the substrate. We also have two forcing terms: $-f_d \nabla \cdot \mathbf{Q}$ the usual term of the stress applied by bacteria, acting as dipoles, in a suspension and $g_0 \vec{p}$, a polar term that comes from the fact that bacteria are able to interact also with the substrate intuitively leading, thanks to their elongated body, to an "entrainment" of the fluid.

Chapter 2

Boltzmann approach for a continuum theory of wet active matter

The Boltzmann-Ginzburg-Landau (BGL) approach has been firstly introduced to derive a continuum theory from the Vicsek model with polar alignment interaction. This method has been then applied to self-propelled rods (dry case) [12] and was able to predict the onset of global nematic order and describe other phenomena observed in simulations of the microscopic model [6]. However, it is clear from the work of H.Li *et al.* [9] that considering explicitly the fluid-particles interaction is essential to properly model bacteria swarming. For this reason a proper continuum theory for such systems need to consider an additional slow variable, the fluid velocity field $\vec{v}$ and its coupling to the particles' density and the polar and nematic fields. To this end, in this chapter I will adapt the BGL approach to include the effect of the fluid when deriving a continuum theory.

2.1 Boltzmann equation

This approach is based on writing a (generalized) Boltzmann equation for the single particle marginal probability density function $f(\vec{r}, \theta, t)$ for a particle being at a given position $\vec{r}$ with a given polarity θ, choosing as normalization constant the total "mass" of the particles $V\rho_0$ where ρ_0 is the mean density.

$$\frac{1}{V}\int_V \mathrm{d}\vec{r}\int_{-\pi}^{\pi}\mathrm{d}\theta f(\vec{r},\theta,t) = \rho_0 \tag{2.1}$$

The Boltzmann equation reads:

$$\frac{\partial f(\vec{r},\theta,t)}{\partial t}+\vec{\nabla}_{\vec{r}}\cdot(f(\vec{r},\theta,t)(s_0\hat{e}(\theta)+\vec{v}(\vec{r})))+\partial_\theta(f(\vec{r},\theta,t)(C_v\omega+C_sF(\mathbf{E},\theta)))=I_{dif}[f]+I_{col}[f] \tag{2.2}$$

The first *streaming* part of the equation (last two terms on the LHS) is composed by the convective mass flux in the position-orientation $(\vec{r}-\theta)$ space due to the fluid and the self-propulsion speed. The streaming rules for position and orientation are eqs. (1.7,1.8) without noise. To lighten the notation we used $\omega=\vec{\nabla}\times\vec{v}$ and $F(\mathbf{E},\theta')=\hat{e}(\theta')\times(\mathbf{E}\cdot\hat{e}(\theta'))\cdot\hat{z}$ and $\hat{e}(\theta)$ is the unit vector with orientation θ.

On the RHS instead we have the self-diffusion integral and the collision integral that takes into account particles' rotational diffusion and a noisy nematic alignment. Note that in this case the Boltzmann equation is coupled to the Stokes equation for the fluid 1.9.

Self-diffusion integral

To evaluate the diffusion integral some assumptions need to be made. In absence of collisions it is assumed that the particle's orientation evolves according to the following stochastic process: particles undergo self-diffusion events with rate λ and when this happens its orientation change by an angle η sampled from a distribution, in this case we assume it to be a Gaussian with zero mean and variance σ^2, $P_\sigma(\eta)$. This leads to the following term:

$$I_{dif}[f]=-\lambda f(\vec{r},\theta,t)+\lambda\int_{-\pi}^{\pi}\mathrm{d}\theta'\int_{-\infty}^{\infty}\mathrm{d}\eta P_\sigma(\eta)\delta_{2\pi}(\theta'-\theta+\eta)f(\vec{r},\theta',t) \tag{2.3}$$

Where $\delta_{2\pi}$ is a 2π periodic delta function that is equivalent to the following:

$$\delta_{2\pi}=\sum_{m=-\infty}^{+\infty}\delta(\theta'-\theta+\eta+2m\pi) \tag{2.4}$$

Collision integral

To evaluate the collision integral we need to make two simplifying assumptions: the first is to consider only binary interactions and the second is the so called *molecular chaos hypothesis* which (for binary collisions only) consists in assuming the factorization of the 2-particle marginal into the product of single particle marginals $f_2(\vec{r}_1,\theta_1,t;\vec{r}_2,\theta_2,t)=f(\vec{r}_1,\theta_1,t)f(\vec{r}_2,\theta_2,t)$.

Furthermore the orientations of two particles colliding evolve according to the following stochastic process, independent from self-diffusion:

$$\theta_1'=\Psi(\theta_1,\theta_2)+\eta_1,\qquad\theta_2'=\Psi(\theta_2,\theta_1)+\eta_2 \tag{2.5}$$

Where η_1, η_2 are two two random variables that in this case we assume to be sampled from the same distribution of self-diffusion $P_\sigma(\eta)$ but in principle they can be different. Because of isotropy $\Psi(\theta_1, \theta_2)$ should also satisfies:

$$\Psi(\theta_1 + \phi, \theta_2 + \phi) = \Psi(\theta_1, \theta_2) + \phi \mod \pi \tag{2.6}$$

Where modulus π is given by the π-symmetry of the particles w.r.t. the interaction (nematic alignment). Eq. (2.6) implies that the interaction function Ψ is parameterized by a single variable function $H(\Delta) := \Psi(0, \Delta)$ since

$$\Psi(\theta, \theta + \Delta) = \theta + \Psi(0, \Delta) \mod \pi \tag{2.7}$$

The collision rate is encoded in the *collision kernel* $K(\Delta = \theta_1 - \theta_2) \geq 0$ that depends only on the angle difference because of the rotational invariance of the problem.
For self-propelled rods the two functions just introduced are $H(\Delta) = \frac{\Delta}{2}$ for $-\pi/2 \leq \Delta \leq \pi/2$ and π-periodic (nematic alignment) while:

$$K(\Delta) = 2v_0 r_0 \left|\hat{e}(\theta_2) - \hat{e}(\theta_1)\right| = 4s_0 r_0 \left|\sin\frac{\Delta}{2}\right| \tag{2.8}$$

In principle the fluid may have an effect on the collision kernel, but we decided to neglect it at this level and utilize the same kernel used in the Dry case. This is evaluated in terms of a scattering process between particles having an isotropic interaction range of radius r_0, eq. 2.8 is the flux of incoming particles through the cross-section $2r_0$ of a target particle.

The collision integral can then be written as:

$$I_{col}[f] = -f(\vec{r}, \theta, t) \int_{-\pi}^{\pi} \mathrm{d}\theta' K(\theta' - \theta) f(\vec{r}, \theta', t) + \int_{-\pi}^{\pi} \mathrm{d}\theta_1 \int_{-\pi}^{\pi} \mathrm{d}\theta_2 \int_{-\infty}^{\infty} \mathrm{d}\eta P_\sigma(\eta) \times K(\theta_1 - \theta_2) f(\vec{r}, \theta_1, t) f(\vec{r}, \theta_2, t) \delta_{2\pi}(\Psi(\theta_1, \theta_2) + \eta - \theta) \tag{2.9}$$

2.2 Angular Fourier transform and order parameters

To derive the dynamics of the slow fields from the Boltzmann equation, we first need to expand f in angular Fourier components, defining:

$$f(\vec{r}, \theta, t) = \frac{1}{2\pi} \sum_{k=-\infty}^{\infty} \hat{f}_k(\vec{r}, t) e^{-ik\theta} \quad \text{where} \quad \hat{f}_k(\vec{r}, t) = \int_{-\pi}^{\pi} \mathrm{d}\theta f(\vec{r}, \theta, t) e^{ik\theta} \tag{2.10}$$

In particular, the first few components are related to the slow variables 1.3 we are interested in: $\hat{f}_0 = \rho$,

$$\hat{f}_1 = \rho(p_x + ip_y), \qquad \hat{f}_2 = \rho(Q_{xx} + iQ_{xy}) \tag{2.11}$$

Hence these Fourier modes can be used as order parameters.

Taking the angular Fourier transform 2.10 of the Boltzmann equation 2.2 an infinite hierarchy of equations is obtained for the $\hat{f}_k$s (the hat is removed in the following to lighten the notation):

$$\frac{\partial f_k}{\partial t} + \frac{s_0}{2}(\nabla f_{k-1} + \nabla^* f_{k+1}) - ikf_k C_v \Im(\nabla^* V) + \frac{C_s k}{4}(f_{k+2}\nabla^* V^* + f_{k-2}\nabla V) + \\ + \Re(\nabla^*(f_k V)) = -(1 - P_k)f_k + \sum_{q=-\infty}^{\infty} (P_k I_{kq} - I_{0q}) f_q f_{k-q} \tag{2.12}$$

Where I_{kq} is defined by the following integral:

$$I_{kq} = \frac{1}{2\pi}\int_{-\pi}^{\pi} \mathrm{d}\Delta K(\Delta) e^{-iq\Delta + ikH(\Delta)} \tag{2.13}$$

and $P_k(\sigma) = \int_{-\infty}^{\infty} \mathrm{d}\eta P_\sigma(\eta) e^{ik\eta}$ that in the case of a Gaussian white noise becomes $P_k(\sigma) = e^{-\frac{\sigma^2 k^2}{2}}$. Except for f_0 that is real thanks to $f_k^* = f_{-k}$ from eq. 2.10 the other fields are complex. When using f_k as fields, the complex notation used in eq. 2.12 is more natural and compact w.r.t. writing directly the equations for the real and imaginary parts. In this notation $\nabla = \partial_x + i\partial_y$, $\nabla^* = \partial_x - i\partial_y$ and $V = v_x + iv_y$ where v_x and v_y are the components of the fluid velocity field. Eqs. 2.12 are coupled to the equation for the fluid 1.9 that in complex notation reads:

$$\mu\Delta V - \nabla P - \alpha V + g_0 f_1 - \frac{f_d}{2}\nabla^* f_2 = 0 \quad \text{with} \quad \Re(\nabla^* V) = 0 \tag{2.14}$$

The equation for k = 0 is just the conservation equation for the total number of particles:

$$\partial_t \rho + s_0 \Re(\nabla^* f_1) + \Re(\nabla^*(\rho V)) = 0 \tag{2.15}$$

First unstable mode

Directly from eqs. 2.12 is possible to study the linear stability of the trivial disordered solution ($\rho = \rho_0$, $f_k = 0$ for $k > 0$ and $\vec{v} = 0$). For $k > 0$ linearizing around this isotropic solution leads to:

$$\partial_t f_k = \mu_k f_k \quad \text{where} \quad \mu_k = [-(1 - P_k) + (P_k(I_{kk} + I_{k0} - (I_{0k} + I_{00}))\rho_0] \tag{2.16}$$

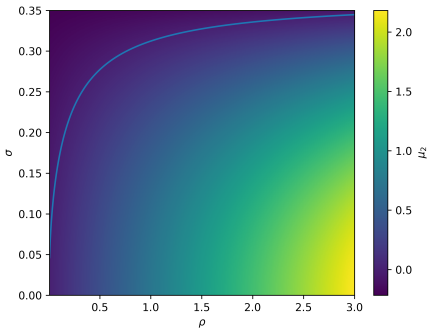

Figure 2.1: Values of μ_2 on a selected region of the phase diagram. The blue line is $\mu_2 = 0$. Above the line, $\mu_2 < 0$, the disordered phase is stable while, below, $\mu_2 < 0$, the ordered solution exists while the disordered one becomes unstable.

In particular, the linear stability of the mode f_k is controlled by the linear coefficient μ_k, we should hence look at their signs in a reasonable interval in the ρ, σ plane. Once fixed the collision kernel (K) and the alignment rule (H) one can compute I_{kq} and P_k for different values of ρ and σ so that also the μ_k can be evaluated for different ks. What is found is that μ_1 and μ_k with $k \geq 3$ are always negative, while μ_2 change sign from negative to positive for low enough noise and/or large enough density as shown in figure 2.1 and hence f_2 is the first unstable mode.

2.3 Scaling Ansatz

The specificity of the BGL approach is to use a systematic scaling ansatz near the instability threshold of the first unstable mode in order to truncate and close the hierarchy (2.12) to a set of equations for the interesting fields. We already derived an equation for ρ (2.15), clearly we want an equation for f_2, but we are also interested in having an equation for f_1 given the polar nature of the particles.

At difference with the scaling already proposed for dry self-propelled rods in [12]:

$$\delta\rho = \rho - \rho_0 \sim \epsilon, \quad \{f_{2k-1}, f_{2k}\}_{k\geq 1} \sim \epsilon^k, \quad \nabla \sim \partial_t \sim \epsilon \tag{2.17}$$

we also need to know how the fluid velocity field scales. To do, let us consider the equation for the fluid (2.14). Substituting the incompressibility condition leads, in complex notation to the following expression for the Laplacian of the pressure:

$$\Delta P = g_0 \Re(\nabla^* f_1) - \frac{f_d}{2} \Re(\nabla^{*2} f_2) \tag{2.18}$$

From which we can deduce that with the polar term ($\Re(\nabla^* f_1)$) being order ϵ^2 from

(2.17) the pressure gradient should be $\nabla P \sim \epsilon$. This means that at leading order equation (2.14) is $-\nabla P - \alpha V + g_0 f_1 = 0$ from which we can infer that

$$V \sim f_1 \sim \epsilon \tag{2.19}$$

2.4 Equations

Thanks to relations (2.17,2.19) a proper scaling for any terms in the hierarchy (eq. 2.12) can be inferred. In line with what was previously done for self-propelled rods in the dry case [12] we decide to truncate our equation at order ϵ^3. In order to *close* the hierarchy to two equations for f_1 and f_2 (in addition to the conservation equation 2.15) we need further considerations.

Firstly, we can note that the equations for f_1 and f_2 at order ϵ^3 are coupled to other fields only through f_3 and f_4 and they only appear coupled to terms order ϵ or in terms of their spatial derivatives. Secondly, having $\mu_3 < 0$ and $\mu_4 < 0$, f_3 and f_4 can be effectively considered "fast" variables relaxing on a time scale much smaller than the one of f_2 and ρ to a value defined by the other fields. Effectively using $|\partial_t f_k| \ll |f_k|$ for $k = 3, 4$ we can "enslave" f_3 and f_4 to ρ, f_1, f_2 and thanks to previous consideration we only need their expression up to order ϵ^2 otherwise substitution would lead to terms of order higher than ϵ^3. Enslaving leads to the following expression for f_3 and f_4:

$$f_3 = \frac{s_0}{2\mu_3}\nabla f_2 - \frac{1}{\mu_3}[P_3(I_{3,1} + I_{3,2}) - (I_{0,1} + I_{0,2})]f_1 f_2 \tag{2.20}$$

$$f_4 = -\frac{1}{\mu_4}(P_4 I_{4,2} - I_{0,2}) f_2^2 \tag{2.21}$$

That can be substituted into the equations for f_1 and f_2 leading to:

$$\frac{\partial \rho}{\partial t} = s_0 \Re(\nabla^* f_1) + \Re(\nabla^*(\rho V)) \tag{2.22}$$

$$\begin{aligned}\frac{\partial f_1}{\partial t} + \frac{s_0}{2}(\nabla^* f_2 + \nabla\rho) - \mathrm{i} f_1 c_v \Im(\nabla^* V) + \frac{c_s}{4} f_1^* \nabla V + \Re(\nabla^*(f_1 V)) = \\ = (\mu_1 + \beta|f_2|^2) f_1 + \zeta f_1^* f_2 + \gamma f_2^* \nabla f_2\end{aligned} \tag{2.23}$$

$$\begin{aligned}\frac{\partial f_2}{\partial t} + \frac{s_0}{2}\nabla f_1 - \mathrm{i}2 f_2 c_v \Im(\nabla^* V) + \frac{\rho c_s}{4}\nabla V + \Re(\nabla^*(f_2 V)) = \\ = (\mu_2 - \xi|f_2|^2) f_2 + \nu\Delta f_2 + k_1 f_1^* \nabla f_2 + k_2 \nabla^*(f_1 f_2) + \tau|f_1|^2 f_2 + k_3 f_1^2\end{aligned} \tag{2.24}$$

$$\mu\Delta V - \nabla P - \alpha V + g_0 f_1 - \frac{f_d}{2}\nabla^* f_2 = 0 \quad \text{with} \quad \Re(\nabla^* V) = 0 \tag{2.25}$$

Importantly, all the coefficients are explicit functions of the microscopic parameters such as in particular ρ and σ.

At this point is interesting to note that, at the level of truncation we used (ϵ^3), the presence of the polar forcing term is responsible for the coupling of the fluid and particles' motion. Without the term $g_0 f_1$ in the forcing the fluid velocity V would scale as ϵ^2 instead of ϵ which implies that all the terms coupling fluid and particles' order would be ϵ^4 and would not appear in the equations effectively leading to a fluid and particles' decoupling (at order ϵ^3) which would result in the dry theory already proposed and studied by [12].

Equation rewritten in terms of the physical filed $\vec{p}$ and $\mathbf{Q}$ are written in appendix A

Chapter 3

Study of the hydrodynamic theory

Now that we have an hydrodynamic theory for the self-propelled rods embedded in a Stokes fluid we can analyze possible solutions to see if this can lead to any new insights and relevant predictions for the chaotic motion of topological defects and active turbulence observed in swarming bacteria colonies. In particular we would also like to evaluate how the fluid modify the behaviour of the equations of dry self-propelled rods analyzed in [12]. To this aim we begin by studying the linear stability analysis of the physically relevant stationary homogeneous solutions to obtain a noise-density phase diagram for this model. We then proceed studying numerically the equation also at the non-linear level.

3.1 Linear stability analysis of homogeneous solutions

3.1.1 Disordered phase

Dropping all time and space derivatives in eqs. (2.22,2.23,2.24) we get:

$$\rho = \rho_0; \quad (\mu_1 + \beta|f_2^{(0)}|^2)f_1^{(0)} = 0; \quad (\mu_2 - \xi|f_2^{(0)}|^2)f_2^{(0)} = 0; \quad \vec{v} = 0 \tag{3.1}$$

The trivial solution, associated to the *disordered phase*, always exists:

$$\rho = \rho_0; \quad f_1^{(0)} = f_2^{(0)} = 0; \quad \vec{v} = 0 \tag{3.2}$$

The linear stability of the disordered solution is related to the linear term μ_2. At difference with the terms ξ, β and μ_1 it changes sign becoming positive for sufficiently low noise and high density. Hence, as shown in figure 2.1, above the blue line the disordered solution is stable while below becomes unstable.

3.1.2 Ordered phase

In the region where μ_2 is positive a second, physically relevant, homogeneous solution exists thanks to the Ginzburg-Landau-like term in equation (2.24), that is:

$$f_2 = \sqrt{\frac{\mu_2}{\xi}}; \quad f_1 = 0; \quad \rho = \rho_0; \quad \vec{v} = 0 \tag{3.3}$$

Taking f_2 real consists in assuming that the order is along x-axis (only the modulus of f_2 is fixed from the equation) which we can do without loss of generality.

What has been done next is the linear stability analysis of the ordered homogeneous solution with respect to non-homogeneous perturbations, namely:

$$\rho(\vec{r},t) = \rho_0 + \delta\rho(\vec{r},t); \quad f_1(\vec{r},t) = \delta f_1(\vec{r},t); \quad f_2(\vec{r},t) = f_2^{(0)} + \delta f_2(\vec{r},t); \quad V(\vec{r},t) = \delta V(\vec{r},t) \tag{3.4}$$

We then substitute these expressions in eqs. (2.22,2.23,2.24) and expand up to first order in the perturbations considering the explicit dependence on the density of the different coefficients up to order ϵ^3 as in the truncation. Note that thank to the absence of time derivatives in the Stokes equation (2.14) and the incompressiblity condition, the small perturbation to the velocity field can be explicitly written in terms of the perturbations of the other fields and substituted in the remaining equations.

We consider then the usual ansatz for the perturbations:

$$\delta\rho(\vec{r},t) = \delta\rho_0 e^{st+i\vec{q}\cdot\vec{r}}; \quad \delta f_1(\vec{r},t) = \delta f_1^{(0)} e^{st+i\vec{q}\cdot\vec{r}}; \quad \delta f_2(\vec{r},t) = \delta f_2^{(0)} e^{st+i\vec{q}\cdot\vec{r}}; \quad V(\vec{r},t) = \delta V^{(0)} e^{st+i\vec{q}\cdot\vec{r}} \tag{3.5}$$

Where the term before the exponentials are assumed to be small, $\vec{q}$ is a wave vector of real components and s is an *a priori* complex growth rate. What we look for is the dispersion relation $s(\vec{q})$, in particular its real part, that if positive for some wavevectors $\vec{q}$ means an instability of the starting ordered solution around which we expanded. At linear order, the ansatz (3.5) leads to the following eigenvalue equation for s:

$$s \begin{pmatrix} \delta\rho \\ \delta f_1^R \\ \delta f_1^I \\ \delta f_2^R \\ \delta f_2^R \end{pmatrix} = M(\rho_0, \sigma, f_2^{(0)}, \vec{q}, ...) \begin{pmatrix} \delta\rho \\ \delta f_1^R \\ \delta f_1^I \\ \delta f_2^R \\ \delta f_2^R \end{pmatrix} \tag{3.6}$$

where M is a five by five matrix and R and I indicate the real and imaginary parts of the respective fields.

We compute numerically the the solutions of Eq. (3.6) that consists in evaluating, at fixed values of all other microscopic parameters, the spectrum of M for different values of ρ, σ and $\vec{q}$. In particular, it consists in computing, for each couple (ρ, σ), in a set spanning the interesting part of the phase diagram (where the

ordered solution exists), the eigenvalues of M in the wave vector space. A positive real part of one of the eigenvalues at some $\vec{q}$ implies an instability of the ordered solution at that point of the phase diagram for a perturbation characterized by that wave vector.

3.1.3 Phase diagram

The results of the linear stability analysis are presented in terms of the density-noise phase diagrams in which the stability of the ordered solution is shown as a function of the mean density ρ_0 and noise σ. For this work we focus in particular on the differences introduced by the fluid with respect to the Dry case, hence we study how the phase diagram depends on different fluid-related parameters (in this work mainly f_d and g_0).

Firstly we reproduced the phase diagram obtained for the dry case in [12], that is equivalent to fix $C_v = C_s = g_0 = f_d = 0$. In figure (3.1) colors indicate the angle between the most unstable wavevector and the direction of nematic order (white for stable regions). Just below the blue line corresponding to $\mu_2 = 0$ there is an intermediate region where the ordered solution exists but it is linearly unstable and the direction of the most unstable wave vector is approximately perpendicular to the direction of the order (transversal instability). Below that the ordered solution becomes again stable up to the darker region in figure (3.1).

Spurious instability

At low enough noise the ordered phase become unstable again. This is a *spurious* instability since it is not observed at the level of the kinetic theory [10], hence it is probably introduced by the truncation procedure which, strictly speaking, is valid only near the order disorder transition line. The nature of such instability was investigated and its presence was connected to the following eigenvalue at $\vec{q} = 0$:

$$\frac{\beta\mu_2 + \mu_1\xi + \zeta\sqrt{\mu_2\xi}}{\xi} \tag{3.7}$$

In the region of existence of the ordered solution the first two terms in the numerator are negative while the second is positive and increases moving toward the bottom right of the phase diagram leading to the instability. This suggests that the instability can be traced back to the term $\zeta f_1^* f_2$ in the equation for f_1 (2.23).

3.1.4 Effect of the fluid

In this section we analyze the phase diagram of the wet model, in particular focusing on the difference with respect to the dry case and the effect of the forcing

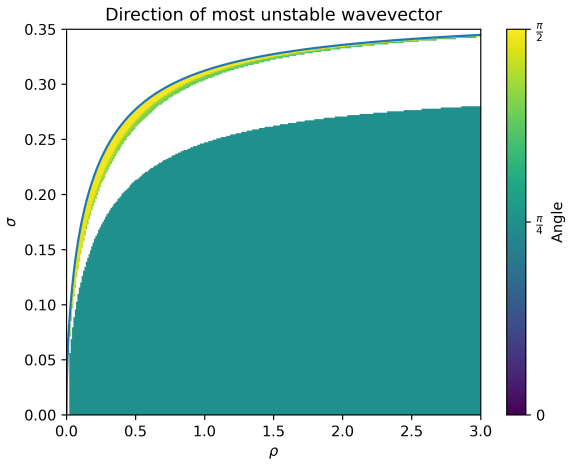

Figure 3.1: Phase diagram from hydrodynamic equation for dry self-propelled rods. In blue the line given by $\mu_2 = 0$ marking the existence of the ordered solution below it. White correspond to stable ordered solution. The color indicates the angle of the most unstable wave vector w.r.t. the direction of the order (x-axis).

parameters f_d and g_0. For everything that will be discussed from now on we fix $C_v = 0.5$ and $C_s = 1$ that are the values computed for perfect ellipsoids [8].

Effect of f_d

The coefficient f_d is related to the force dipoles that the bacteria are known to exert on the fluid. The sign in particular is related to the existence of two main types of bacteria with respect to how the fluid is put in motion around each of them: *pushers* and *pullers* corresponding respectively to positive and negative values of f_d. The names comes from how the fluid is put in motion with respect to their elongated direction: pushers "push" the fluid away from them along their elongated direction and aspirating it along the short direction while pullers are characterized by the opposite dipole. What is currently understood is the fact that, high level of activity (high $|f_d|$ in our context) destabilizes the nematically ordered phase in both cases (see figure (3.2).

What is observed for positive values of f_d (pushers) is that indeed the active forcing on the fluid destabilizes the ordered solution. From figure (3.4, left column) we see that at high enough density (depending on the value of f_d) a longitudinal (the most unstable wavevector is parallel to the direction of nematic order) instability of the ordered solution appears. Increasing f_d the threshold density over which the instability appears decreases, in other words the "new" unstable region expands from the the high to the low density side of the phase diagram.

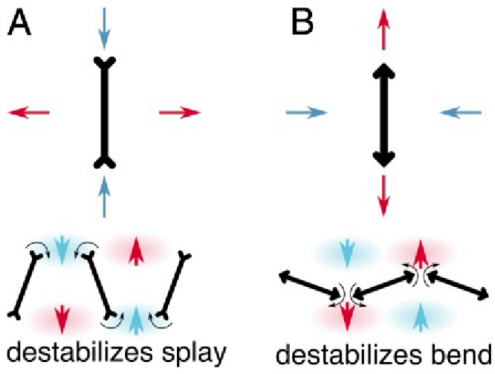

Figure 3.2: Illustration of how the fluid flow around pullers (A) and pushers (B) destabilizes respectively *splay* and *bend* perturbations leading to an unstable nematically ordered phase. Adapted from [11].

On the other hand (figure 3.4 right column) for negative values of f_d (pullers) the ordered solution is not destabilized for the same values of $|f_d|$ at which we see the appearance of the new unstable region for pushers.

Effect of g_0

At fixed values of f_d, increasing the positive value of g_0 have a similar effect as increasing a positive value of f_d: the new instability region further expand in the low density side of the phase diagram (figure 3.3)

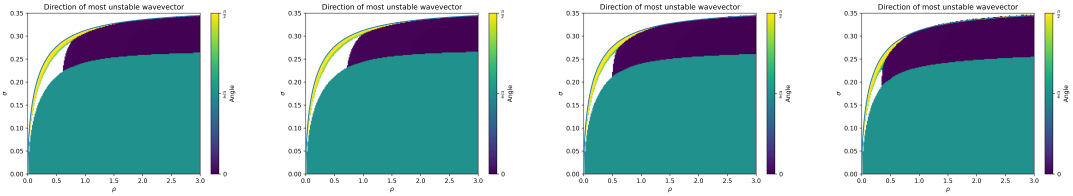

Figure 3.3: Effect of g_0 on the phase diagram: the plot are produced with increasing positive values of g_0 from left to right, respectively $g_0 = 1,\ 5,\ 10,\ 20$. f_d is fixed to 10 while all the other parameters are the same as figure (3.4). Increasing the value of g_0 a wider region of the phase digram becomes unstable.

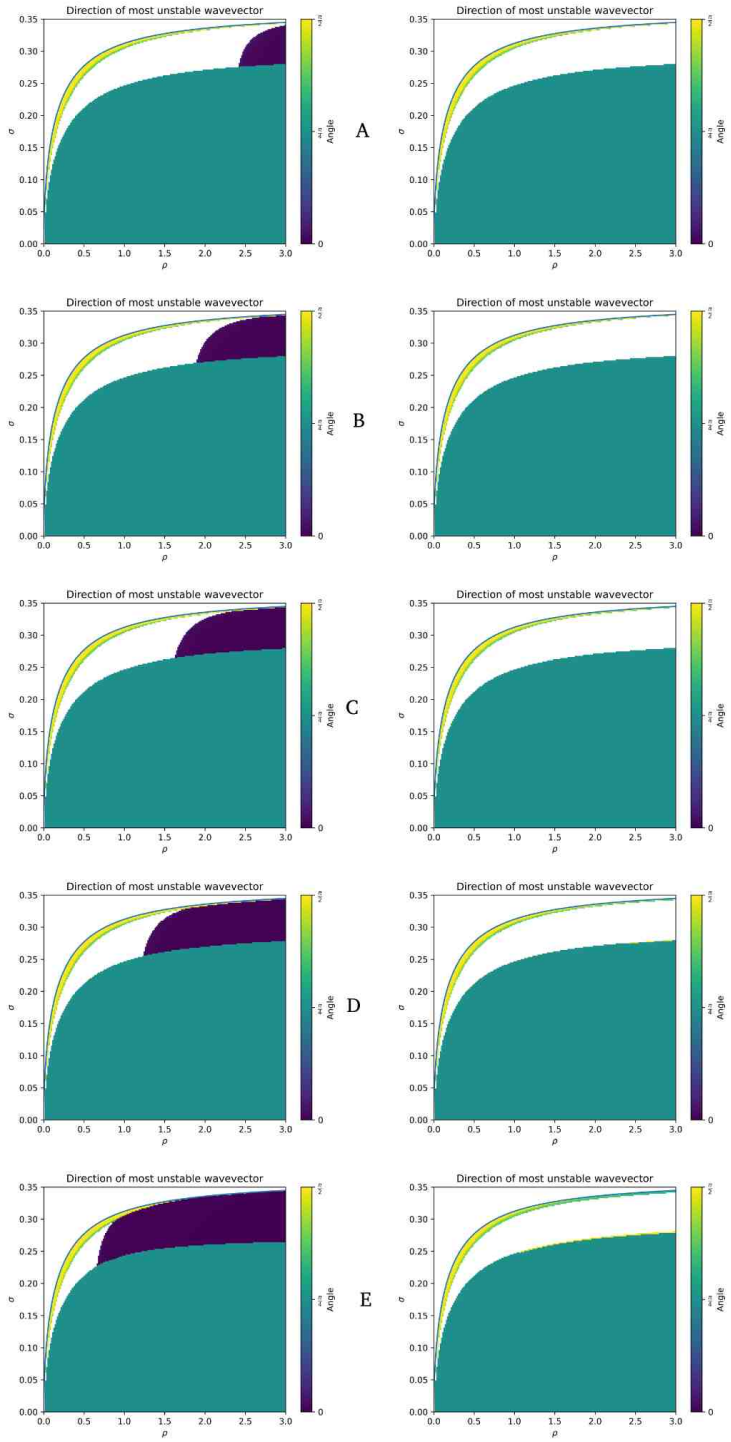

Figure 3.4: Phase diagrams from linear stability analysis. In each row there two phase diagrams for opposite values of f_d *left* column for positives while the *right* one is for the negatives. $|f_d|$ is: (A) 0.2, (B) 0.6, (C) 1.0, (D) 2.2, (E) 10. Color code and axis values as in figure (3.1). In these phase diagram the fluid related parameters are fixed to be: $\mu = 200$, $\alpha = 10$

3.2 Numerical integration of the PDEs

To see how the equations behave at the full non-linear level a numerical integration is required because of the complexity of this system of PDEs. In this work, in particular, we are interested in checking if the model derived is capable of reproducing the bacterial turbulence and the chaotic motion of topological defects observed in active nematics [9]. These phenomena are all observed in the bulk of the colony, hence the bulk behaviour is our main interest.

Because of this, we decided to integrate the PDEs numerically on a square domain with Periodic Boundary Conditions (PBC) using a pseudo-spectral method. This has been practically performed with a `Julia` code written from scratch by me and described in more details in Apppendix B. We now discuss the numerical solutions of the equations with a particular focus on the differences and similarities with respect to the dry case. We would also like the reader to know that what we have been able to perform so far is a preliminary analysis of the simulations which allows us only to remain on a qualitative level regarding the considerations we will do in the following.

3.2.1 Dry non-linear equations

Firstly, I used my code to check the phenomenology observed in [12] for the non-linear equations for the dry model. These corresponds to eqs. (2.22,2.23,2.24) without the terms involving the fluid velocity V.

The Dry case is characterized by two main types of behaviours, ignoring the spurious instability region. The first is the existence of band solutions in a region that corresponds approximately with the linear instability region just below the order-disorder transition line (see phase diagram (3.1)). These bands are nematically ordered and are stable for systems small enough while for large enough systems they become unstable and move in a chaotic way, as also found by simulations of the microscopic model [6] (figure 1.8). The bands can be obtained integrating the equations deterministically starting from slightly non-homogeneous conditions in the linear instability region. Bands also exists in a region slightly wider and they can be observed when integrating from initial conditions that are inhomogeneous enough (bands-like) outside the instability region at both higher and lower levels of noise. A snapshot from a typical simulation showing bands is in figure (3.5).

Already at this level is possible to observe the presence of defects whose mobility and lifetimes depends on the their type (+1/2 and -1/2) and on the noise level.

Starting from a slightly non-homogeneous condition but integrating at values of ρ and σ deeper in the stable region what we get is the formation of defects that move relatively slower, while the system is relaxing towards the homogeneous

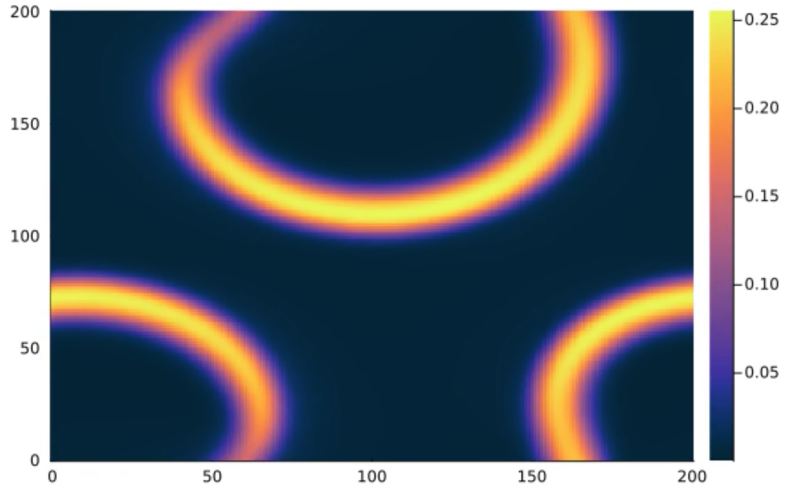

Figure 3.5: Snapshots taken from a typical simulation of the Dry model in the band regime. In color the modulus of the complex nematic field f_2, to show the nematic order found in the bands. Obtained integrating from a band-like starting point for $\rho = 0.65$ and $\sigma = 0.2949$

stable state.

3.2.2 Wet non-linear equations

When integrating deterministically the hydrodynamic equations for the wet model some of the features that have been observed for the dry model are sill present: bands solutions exist in transversal instability region but their domain of existence have not been studied in details yet.

The model behave in a new, interesting way in the longitudinal instability region of the phase diagram introduced by the fluid coupling to the particles' motion. In this region, that we recall, it is found only for positive values of f_d, we typically observe structures as those shown in figure (3.6). This new region is characterized by the presence of many defects that move in a chaotic way as observed experimentally and from the microscopic model developed in [9]. By eye the motility of the three-fold rotationally symmetric $-\frac{1}{2}$-defects appears to be smaller with respect to $+\frac{1}{2}$-defects as also observed in [9]. The structures are also reproduces exactly in the density field while f_1 is typically 1 or 2 order of magnitude smaller than ρ and f_2 during all the simulations (Appendix B).

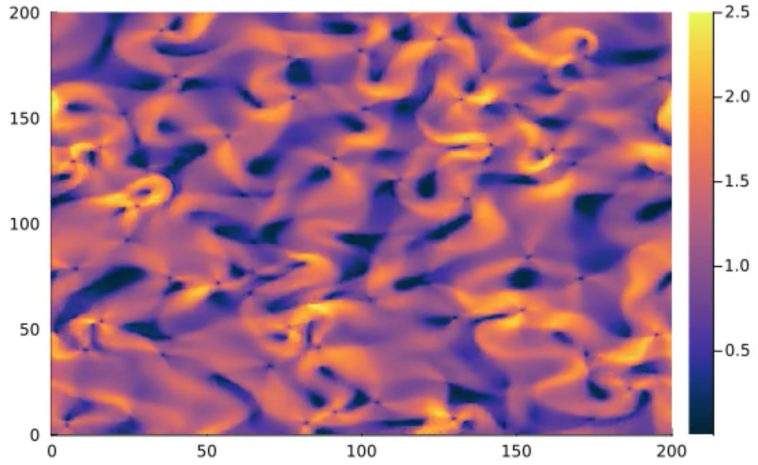

Figure 3.6: Snapshot of $|f_2|$ from a typical simulation in the "new" unstable region introduced by the coupling with the fluid. Integrating deterministically the full equations starting from a slightly inhomogeneous condition on a 200x200 square domain. $\rho = 2.2$, $\sigma = 0.3$, $f_d = 10$, $g_0 = 3$. We can observe topological defects of different signs moving in a chaotic way resembling an active nematics scenario.

For what concerns the fluid motion, the vorticity field for a typical simulation is shown in figure (3.7). A quantitative analysis is still to be done, but from a qualitative point of view we can observe the presence of structures in the vortcity field compatible with an active turbulence scenario. Furthermore the vorticity around the defects appears to be compatible with what observed in [7].

Increasing the positive value of g_0 has the effect, qualitatively speaking, to increase the motility of the defects as we expect from any increase of the forcing terms. The same phenomenology is also observed increasing the average density at which we simulate. Since the forcing terms are proportional to f_1 and f_2 and both these fields are proportional to density is easy to understand the increased motility of the defects in terms of increased forcing also in this case.

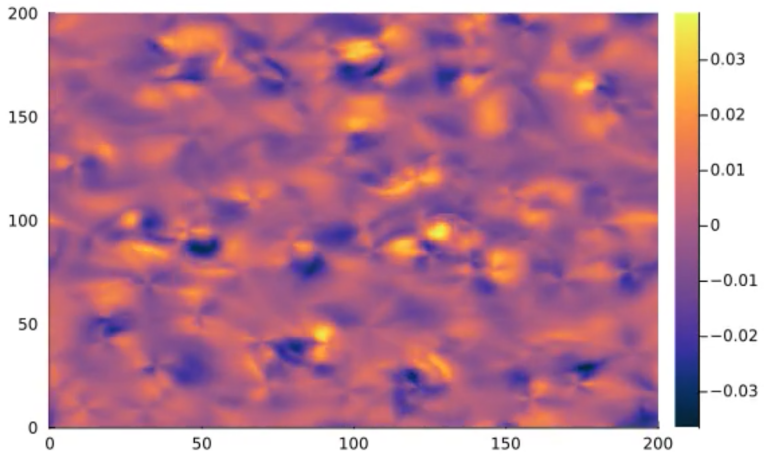

Figure 3.7: Typical snapshot of vorticity field obtained in the same conditions as figure (3.6).

Chapter 4

Discussion and future perspectives

In chapter 2 we derived a continuum theory from a microscopic model of swarming bacteria colonies while in chapter 3 we started their study by performing a linear stability analysis of the stationary homogeneous solutions. Preliminary qualitative observations coming from numerical integration of the PDEs ware also presented in section 3.2.2.

Deriving the Hydrodynamic theory (2.22,2.23,2.24) coupled to the Stokes equation (2.14) we discovered that the polar forcing term ($g_0 f_1$) is responsible for a coupling (at order ϵ^3 of truncation) of particles' and fluid motion.

For pushers ($f_d > 0$), at the linear stability level, the phase diagram is found to be modified with respect to the dry case by the presence of a new unstable region far from the spurious instability in the region of the phase diagram predicted to be stable in the dry model.

Preliminary simulations of the full non-linear equations in the new unstable region suggest that chaotic behavior of the topological defects may be explained to some extent by the model derived in this work. Further quantitative investigations of the equations are planned in order to study the statistical properties predicted by this model to compare with experimental data and microscopic models' simulations performed in [9].

Concerning the possible applications of this work we would like to briefly discuss future research perspectives. The work has been motivated by new experimental observations, made on bacterial swarms, concerning (what appears to be) topologically protected edge currents in weakly chiral bacterial colonies that will appear in a forthcoming paper. Preliminary microscopic simulations, in particular, suggested that such phenomena could be explained by a microscopic model similar to our microscopic starting point.

The study of these (possibly) topologically protected edge modes in such a soft

active living system will be the focus of my PhD project. To this end we believe an hydrodynamic theory derived from a faithful microscopic model is a first step for a theoretical understanding of topological protection in this context. This work, indeed, was aimed at performing a preliminary analysis of a possible continuum theory of wet active matter derived via the Boltzmann-Ginzburg-Landau approach in order to anticipate the future generalizations of this model needed in the context of the new experimental observations.

Bibliography

[1] Ricard Alert, Jaume Casademunt, and Jean-François Joanny. Active turbulence. *Annual review of condensed matter physics*, 13:143–170, 03 2022.

[2] M. Ballerini, N. Cabibbo, R. Candelier, A. Cavagna, E. Cisbani, I. Giardina, V. Lecomte, A. Orlandi, G. Parisi, A. Procaccini, M. Viale, and V. Zdravkovic. Interaction ruling animal collective behavior depends on topological rather than metric distance: Evidence from a field study. *Proceedings of the National Academy of Sciences*, 105:1232–1237, 01 2008.

[3] Avraham Be'er and Gil Ariel. A statistical physics view of swarming bacteria. *Movement Ecology*, 7, 03 2019.

[4] Bengt Fornberg. *A Practical Guide to Pseudospectral Methods*. Cambridge University Press, 1996.

[5] Delphine Geyer, David Martin, Julien Tailleur, and Denis Bartolo. Freezing a flock: Motility-induced phase separation in polar active liquids. *Physical Review X*, 9, 09 2019.

[6] Francesco Ginelli, Fernando Peruani, Markus Bär, and Hugues Chaté. Large-scale collective properties of self-propelled rods. *Physical Review Letters*, 104, 05 2010.

[7] Luca Giomi. Geometry and topology of turbulence in active nematics. *Physical Review X*, 5, 07 2015.

[8] George Barker Jeffery. The motion of ellipsoidal particles immersed in a viscous fluid. *Proceedings of the Royal Society of London. Series A, Containing Papers of a Mathematical and Physical Character*, 102:161–179, 11 1922.

[9] He Li, Xia-qing Shi, Mingji Huang, Xiao Chen, Xiao, Chenli Liu, Hugues Chaté, and Hepeng Zhang. Data-driven quantitative modeling of bacterial active nematics. *Proceedings of the National Academy of Sciences of the United States of America*, 116:777–785, 12 2018.

[10] Benoît Mahault. Outstanding problems in the statistical physics of active matter, 08 2018.

[11] Ananyo Maitra, Pragya Srivastava, M Cristina Marchetti, Juho S Lintuvuori, Sriram Ramaswamy, and Martin Lenz. A nonequilibrium force can stabilize 2d active nematics. *Proceedings of the National Academy of Sciences of the United States of America*, 115:6934–6939, 06 2018.

[12] Anton Peshkov, Igor S Aranson, Eric Bertin, Hugues Chaté, and Francesco Ginelli. Nonlinear field equations for aligning self-propelled rods. *Physical Review Letters*, 109, 12 2012.

[13] Gabriel S. Redner, Michael F. Hagan, and Aparna Baskaran. Structure and dynamics of a phase-separating active colloidal fluid. *Physical Review Letters*, 110, 01 2013.

[14] Volker Schaller, Christoph Weber, Christine Semmrich, Erwin Frey, and Andreas R. Bausch. Polar patterns of driven filaments. *Nature*, 467:73–77, 09 2010.

[15] Alexandre Solon, Hugues Chaté, and Julien Tailleur. From phase to microphase separation in flocking models: The essential role of nonequilibrium fluctuations. *Physical Review Letters*, 114, 02 2015.

[16] John Toner and Yuhai Tu. Long-range order in a two-dimensional dynamicalxymodel: How birds fly together. *Physical Review Letters*, 75:4326–4329, 12 1995.

[17] Tamás Vicsek, András Czirók, Eshel Ben-Jacob, Inon Cohen, and Ofer Shochet. Novel type of phase transition in a system of self-driven particles. *Physical Review Letters*, 75:1226–1229, 08 1995.

[18] Xiaolu Wang, Martin In, Christophe Blanc, Alois Würger, Maurizio Nobili, and Antonio Stocco. Janus colloids actively rotating on the surface of water. *Langmuir: the ACS journal of surfaces and colloids*, 33:13766–13773, 12 2017.

Appendix A

Equations in terms of physical fields

We have also rewritten the hydrodynamic theory using the more commonly used fields: the polar vector field $\vec{p}$ and the nematic tensor field $\mathbf{Q}$ defined in 1.3. In particular since both f_1 and f_2 are proportional to the density ρ as in eq. (2.11) we use the following version of physical fields proportional to ρ:

$$\vec{m} = \rho\vec{p} \quad \mathbf{D} = \rho\mathbf{Q} \tag{A.1}$$

The complex fields hence are equivalent to:

$$f_1 = m_x + \mathrm{i}m_y \quad f_2 = D_{xx} + \mathrm{i}D_{xy} \tag{A.2}$$

Furthermore, we make use of the vorticity and rate of strain tensor respectively defined as (where v_α is a generic component of the fluid velocity field ($\vec{v}$)):

$$\Omega_{\alpha\beta} = \frac{1}{2}(\partial_\alpha v_\beta - \partial_\beta v_\alpha) \quad \mathrm{E}_{\alpha\beta} = \frac{1}{2}(\partial_\alpha v_\beta + \partial_\beta v_\alpha) \tag{A.3}$$

In this notation the equations read:

$$\partial_t + \nabla \cdot [s_0\vec{m} + \rho\vec{v}] = 0 \tag{A.4}$$

$$\partial_t m_\alpha + \frac{s_0}{2}\partial_\beta D_{\alpha\beta} + \frac{s_0}{2}\partial_\alpha \rho + 2C_v\Omega_{\alpha\beta}m_\beta - \frac{C_s}{2}E_{\alpha\beta}m_\beta = (\mu_1 + \frac{\beta}{2}D_{ij}D_{ij})m_\alpha + \zeta D_{\alpha\beta}m_\beta + \gamma\left[\partial_\gamma(D_{\alpha\beta}D_{\beta\gamma}) - D_{\alpha\beta}\partial_\gamma D_{\beta\gamma}\right] \tag{A.5}$$

$$\partial_t D_{\alpha\beta} + \frac{s_0}{2}\left[\partial_\beta m_\alpha + \partial_\alpha m_\beta - (\nabla\cdot\vec{m})\delta_{\alpha\beta}\right] + 2C_v\Omega_{\alpha\gamma}D_{\gamma\beta} + \frac{C_s\rho}{4}(E_{\alpha\beta} - \nabla\cdot\vec{v}\,\delta_{\alpha\beta}) =$$
$$(\mu_2 - \xi\frac{D_{ij}D_{ij}}{2})D_{\alpha\beta} + \nu D_{\alpha\beta} + k_1\left[m_\alpha\partial_\alpha D_{\beta\gamma} + m_\alpha\partial_\beta D_{\alpha\gamma} - m_\alpha\partial_\beta D_{\beta\gamma}\right] +$$
$$k_2\left[\partial_\alpha(m_\alpha D_{\beta\gamma}) + \partial_\alpha(m_\beta D_{\alpha\gamma}) - \partial_\alpha(m_\beta D_{\beta\gamma})\right] + \tau|\vec{m}|^2 D_{\alpha\beta} + k_3(2m_\alpha m_\beta - |\vec{m}|^2\,\delta_{\alpha\beta}) \tag{A.6}$$

Coupled to the Stokes equation for the fluid:

$$\mu\nabla^2\vec{v} + \nabla P - \alpha\vec{v} + g_0\vec{m} - f_d\nabla\cdot\mathbf{D} = 0 \quad \text{with} \quad \nabla\cdot\vec{v} = 0 \tag{A.7}$$

Appendix B

Numerical integration details

The system of PDEs derived in this work has been simulated using a `Julia` code written from scratch. The code implements what is called a pseudo-spectral method for integrating non-linear PDEs using the Fast Fourier Transform. The FFT package used was FFTW thanks to the existing bindings to this library available in Julia.

Taking the Fourier transform of the PDEs we get a system of ODEs for the Fourier components of the different fields. These ODEs are then integrated with a simple explicit Euler time-stepping method. The difficulty in this procedure comes from the presence of non-linear terms that couples different components together. At each time step indeed is necessary to transform back in the field in real space to compute all the non-linear (interaction) terms and transform them back to Fourier space to update the Fourier components.

When computing the non-linear terms we are faced with the *aliasing* problem. Given that our numerical approach fix the resolution of our fields at a given number of modes, when multiplying two expansions together we generally end up with quantities having more non-zero components than those resolved by the code. Numerically speaking, this "high-energy" components contributes, thanks to the FFT algorithm, to the slow modes in a spurious way giving rise to the so-called aliasing.

To solve this problem, anti-aliasing technique has been devised [4]. Essentially they consists in fixing to zero part of the modes (usually $\frac{1}{3}$ for a square non-linearity) after performing any procedure introducing aliasing errors or equivalently updating only a subset ($\frac{2}{3}$) of the modes at each time step. This is what has been implemented in the code. In the code, this so-called $\frac{2}{3}$-rule has been used and independently of the non-linearity at hand.

Typical evolution in time of the average field are shown in figure B.1.

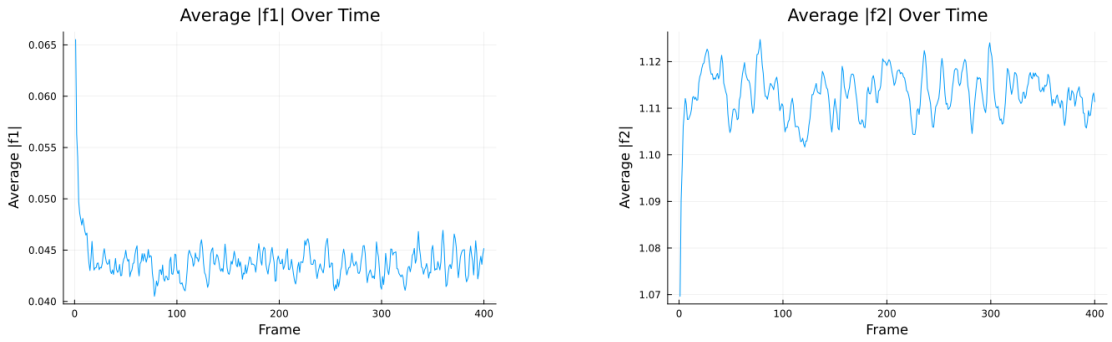

Figure B.1: Time evolution of the average values of $|f_1|$ and $|f_2|$ for the 400 snapshots saved snapshots of a total simulated time T = 20 000. f_1 is significantly lower than f_2 in the stationary regime.